Dynamics of interaction between dislocations and point defects in bcc iron

Luis Casillas-Trujillo, Andrew S. Ervin, Liubin Xu, Alexander Barashev, and Haixuan Xu

Phys. Rev. Materials **2**, 103604 — Published 29 October 2018

DOI: 10.1103/PhysRevMaterials.2.103604

Dynamics of Interaction between Dislocations and Point Defects in bcc Iron

Luis Casillas-Trujillo[1], Andrew S. Ervin[1], Liubin Xu[1], Alexander Barashev[2], Haixuan Xu[1,2*]

[1] Department of Materials Science and Engineering, University of Tennessee, Knoxville, TN 37996 USA

[2]Joint Institute for Advanced Materials, Knoxville TN 37996 USA

*** Email: xhx@utk.edu**

Abstract

The interaction between dislocations and point defects is crucial for many physical properties and phenomena in materials, such as strengthening mechanisms, dislocation bias and void swelling, creep, and impurity segregation around dislocations. Conventional dislocation-point defect interaction models use approximations based on elasticity theory and/or based on assumptions that transition states energies can be deduced from the binding energies of the defects. In this paper, we present the transport properties of point defects near dislocations based on the actual saddle point configuration of vacancies and self-interstitial atoms as a function of position with respect to screw and edge dislocations in a model system (bcc iron) using the self-evolving atomistic kinetic Monte Carlo (SEAKMC). KMC simulations reveal defect dynamics near dislocations are highly anisotropic and correlated, particularly for dumbbells in the compressive field of the edge dislocation, which could result in zones near dislocation cores where dumbbells are less efficiently absorbed compared with vacancies. This study provides accurate saddle point configurations and energies required to properly describe the dynamics of point defects around dislocations, allowing fundamental insights on the transport mechanisms which are essential for understanding microstructural evolution and mechanical properties of metallic materials.

1. Introduction

The dislocation-point defect interaction (DPDI) has a strong impact on the microstructural evolution and plasticity of materials [1-6], including behavior such as impurity segregation around dislocations and creep. The DPDI has two interrelated aspects. On one hand, the presence of point defects near dislocations may influence dislocation properties. For instance, point defects could act as obstacles to dislocation glide [7] or alter the structure of the dislocation core [8], leading to strengthening and hardening. In addition, the absorption or emission of point defects controls dislocation motion through creating kinks and jogs [9] and dislocation creep at low stresses by influencing the dislocation climb processes [10]. On the other hand, the strain field exerted by dislocations affects the migration of point defects, and causes a drifted and correlated diffusion of point defects around dislocations in alloys [11,12]. This drifted diffusion leads to the formation of defect clusters and to the segregation of impurity atoms near dislocations, forming the so-called Cottrell atmospheres [11].

The effects of the DPDI are enhanced in radiation environments [13,14] and by high temperatures, where collision cascades introduce a large number of point defects and point defect mobility is enhanced, respectively. Radiation effects such as void swelling [15], radiation induced segregation [16,17], radiation-induced creep [18], and radiation induced embrittlement/hardening [5,15,19-21] are controlled by the underlying atomistic interactions between point defects and dislocations. Therefore, understanding the mutual interaction between point defects and dislocations is essential to control the mechanical properties and performance of structural materials and to tailor their radiation resistance for nuclear energy applications. In addition, a fundamental understanding of the DPDI may also contribute to fields where defects dominate the materials performance, such as solid oxide fuel cells and batteries [22,23].

Compared with our understanding of defect stability near dislocations based on defect formation energies and binding energies [24], relatively little is known about the transport properties and dynamics of point defects in the presence of a dislocation. One of the difficulties is to determine the saddle point energies (SPs) and corresponding migration energy barriers (MEB) in a systematic way, which is rather complicated and computationally demanding. Bilby [25] and Cottrell [26] provided the first description of the DPDI using elasticity theory, by considering the elastic interaction of the strain field of the dislocation and the strain introduced by the dilatation volume of the point defect to reach approximate solutions. Another commonly used approximation is to estimate the MEBs based on the binding energies of point defects. This approximation has been commonly used to study the DPDI [27-30] . It should be noted that both the Bilby-Cottrell model and the binding energy approximation are based on properties of

local minimum configurations in the potential energy landscape, and no information of the transition state is considered.

In principle, a single MEB can be computed using the drag [31], nudged elastic band (NEB) [32,33] or the dimer [34] methods, but until now it has been computationally prohibitive to calculate the SP configuration for all the different local atomic configurations caused by the presence of dislocations. The usage of these transition state search algorithms is limited when the number of degrees of freedom is high [35]. To overcome this limitation, attempts involving artificial neural networks [36-38], and genetic algorithms [39] have been made. In these methods, they use training sets to predict the SP energy of different local atomic configuration without obtaining the actual MEBs. These artificial intelligence methods are promising but strongly depend on having a proper training set and require an *a priori* knowledge of hundreds of thousands of SP energies.

In this work, we have taken advantage of the recently developed Self-Evolving Atomistic Kinetic Monte Carlo (SEAKMC) [35,40-43] method with improved algorithm and efficiency to systematically calculate the actual SP energies as a function of position with respect of the dislocation core for vacancies and the family of <110> self-interstitial atom (SIA) dumbbells in the presence of a single straight screw or edge dislocation in bcc iron. The rest of the paper is organized as the following, the system setup and computational details are given in section 2. The results of this study are presented in section 3. First we present the saddle point configuration of point defects in bulk bcc iron in section 3.1, the results for the screw dislocation in section 3.2, and edge dislocation in 3.3. We examine the anisotropy of diffusion in section 3.4. We employ the obtained data to perform kinetic Monte Carlo simulations (KMC) and study point defect trajectories in section 3.5. The results for the different types of defects and dislocations are compiled in the Supplementary Material. Section SM1 Contains the results for a vacancy near a screw dislocation, section SM2 a vacancy near an edge dislocation, SM3 a dumbbell near a screw dislocation, SM4 a dumbbell near an edge dislocation and SM5 the anisotropy of diffusion.

2. Simulation Setup and Computational Details

2.1 Dislocation Models

The screw dislocation has a Burgers vector ½ <111>, and the dislocation line lies in the [111] direction in bcc iron. The initial screw dislocation structure was created by displacing the atoms according to linear isotropic elasticity theory [9,44] and subsequently relaxed using interatomic potentials to obtain a stable configuration. The geometric center of the screw dislocation should be aligned to a point of those with 3-

fold symmetry. Particularly, we used the Ackland potential of bcc iron [45] since it gives the correct description of the dislocation core [46].

The Burgers vector of the edge dislocation is ½[111] with slip plane $(1\bar{1}0)$, and dislocation line direction is $[11\bar{2}]$. The edge dislocation was created by the procedure described by Ossetsky *et al*. [47]. The perfect crystal is divided in two halves. Initially, we have equal number of planes in the upper and lower crystals. Planes within one spacing b in the lower part of the crystal are removed. In the lower half of the crystal the length in the Burgers vector direction becomes *(N-1)*b*. The one-plane mismatch tends to bend the crystal out of the rectangular shape. For practical simulations, however, the crystal must be constrained to remain rectangular, so a periodical boundary condition can be applied. This constrain introduces extra stress to the dislocation. To minimize this effect the upper crystal is shrunk by *–b/2* in the y direction and the lower elongated by *+b/2* according to [47]. In Fig. 1, we show the coordinate system for both screw and edge dislocations, and the projection on the plane perpendicular to the dislocation line, where we show the migration directions and the first and second nearest neighbors.

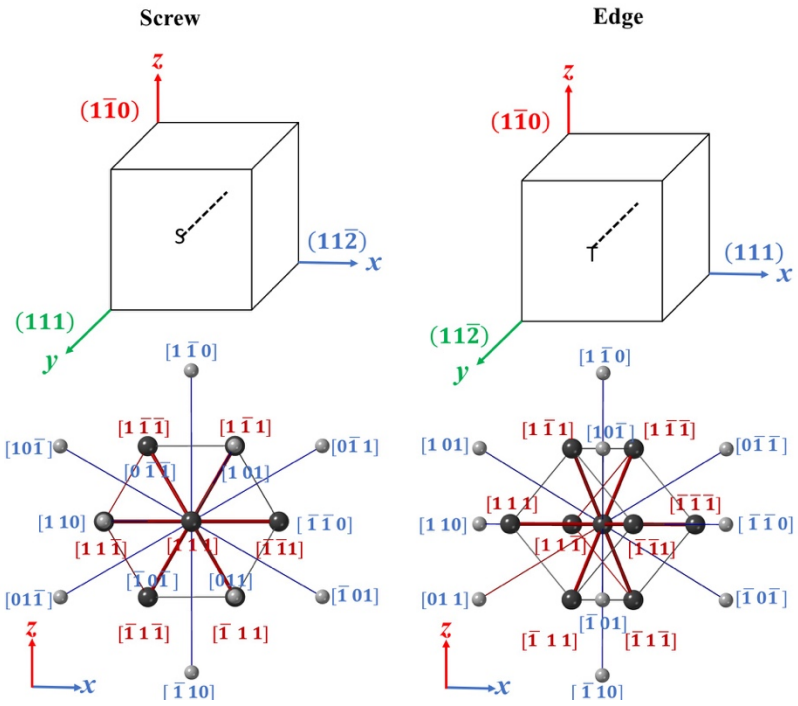

Figure 1: The upper portion of the figure shows the coordinate systems used for screw and edge dislocations. The dislocation line for both dislocations is along the *y* direction. The lower portion of the figure shows a projection of the plane perpendicular to the dislocation line, the first nearest neighbors are shown as black atoms, and the second nearest neighbors as small silver atoms. The <111> migration directions are shown with thick red lines, and the <110> directions with thin blue lines.

2.2 Simulation Setup

The geometry of the simulation box is a rectangular parallelepiped with the axis of $\langle 111 \rangle$, $\langle 110 \rangle$, and $\langle 112 \rangle$. These directions are chosen based on the slip system of bcc iron. In particular, we chose the (111), $(11\bar{2})$ and $(1\bar{1}0)$ directions. The dislocation line was assigned to the *y* direction and the $(1\bar{1}0)$ direction was assigned to *z*. The block of atoms has been made infinite in the *x* and *y* directions by applying periodic boundary conditions, thus having an infinitely long dislocation, and an infinite array of parallel dislocations. The dimension of our crystal was chosen to minimize the interaction between image dislocations such as at the boundary of the box where the strain field is negligible. The system sizes for both screw and edge dislocations are given in Table 1, and Fig. 2 shows a schematic of the simulation cell for and edge dislocation.

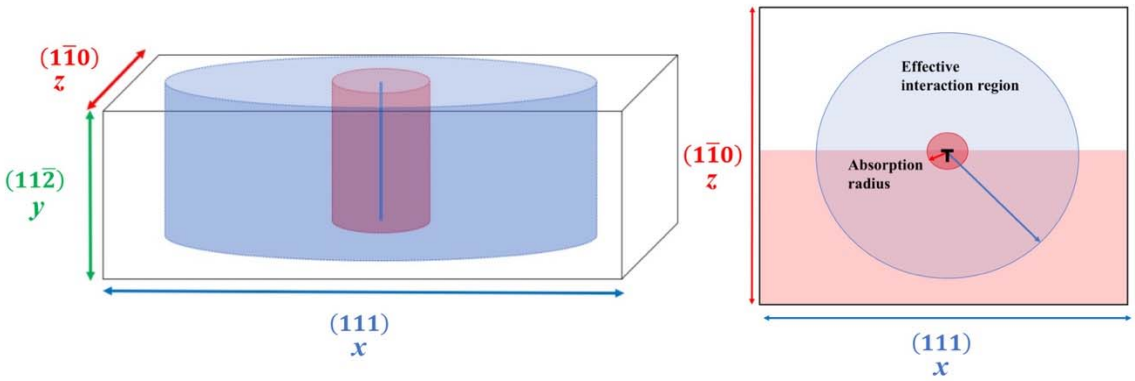

Figure 2: (a) Simulation cell used in this study for edge dislocation. (b) Top view of the simulation cell.

Table 1. Simulation system size.

Simulation box size				
	x<112>(Å)	y<111>(Å)	z<110>(Å)	Number of atoms
Edge	227	35	226	153720

Screw	210	40	200	144000

To investigate the DPDI we have chosen atoms within a certain radius (R) to the dislocation line, and have denominated this region as the "effective interaction region". Systematically we investigated one defect at a time within this effective interaction region. We have studied a vacancy and a $\langle 110 \rangle$dumbbell since it is the most stable interstitial defect in bulk iron. We have calculated the SP energies for all the $\langle 1\bar{1}0 \rangle$ dumbbell configuration: $[110], [101], [011], [\bar{1}10], [\bar{1}01]$ and $[0\bar{1}1]$. After the introduction of each defect, the system is relaxed and then the SP search is performed.

2.3. Saddle Point Searches using SEAKMC.

We have performed the SP search using SEAKMC. SEAKMC is an atomistic on-the-fly KMC method [35,42]. On-the-fly refers to the fact that SP configurations and energies are determined as the system evolves. SEAKMC focuses on defect interaction and evolution with atomistic fidelity and only requires an input structure and interatomic potential as input without assuming potential defect migration mechanisms and energies. SEAKMC utilizes the Dimer method [48,49] to search the SP directly without knowledge of the final state *a priori*. The Dimer method is based on the harmonic approximation of transition state theory (HTST) [34,50]. We have used the SP configuration of the bulk of each defect as a starting guess of the SP configuration in the presence of a dislocation, which results in a multiple order of magnitude of improvement in the SP search efficiency. The SP energy was determined to a precision of 1meV.

3. Results and Discussions

3.1 Saddle Point Sampling of Point Defects in the Bulk BCC Iron

First, we have calculated SP configurations in bulk bcc iron for vacancies and dumbbells. The SP searches for a vacancy predominately result in eight SPs associated with first nearest neighbor jumps, located along the <111> directions (Fig. 3a). Comparatively, the SP distribution around a <110> interstitial dumbbell (Fig. 3b) is much more complicated than the vacancy case. Several sets of SPs that correspond to different transition states are found, including two different sets that correspond to first nearest neighbor migrations with a translation-rotation mechanism. Of these first nearest neighbor migrations, one set corresponds to the nearest neighbors that lie in the direction of the dumbbell and the other set to migrating to the neighbor perpendicular to the dumbbell. Besides first nearest neighbor

migrations we found SPs that correspond to pure rotations, one set of SPs to a <111> crowdion and one set to <110> rotations.

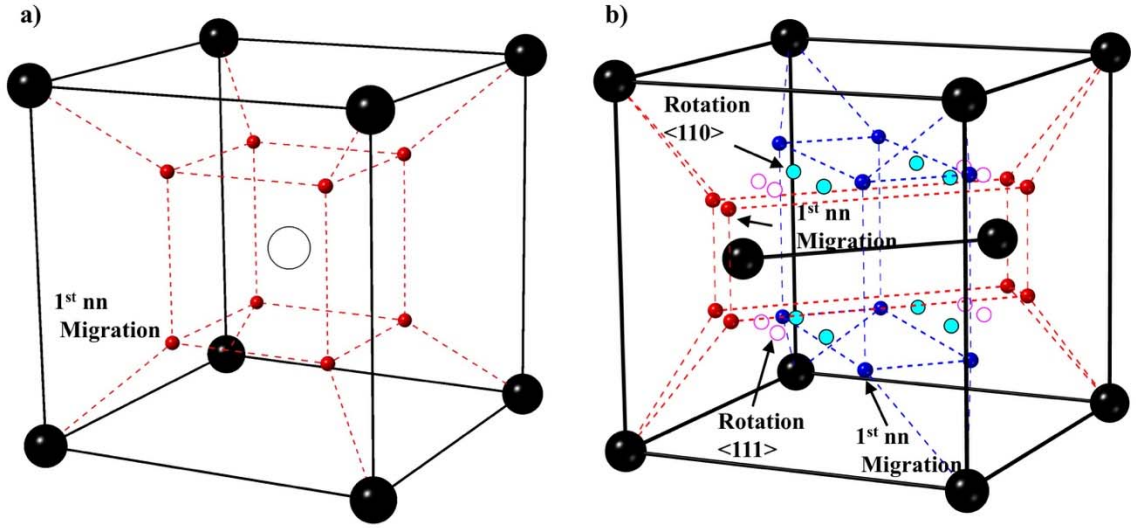

Figure 3: SP configuration in bulk Fe for (a) vacancy (b) <110> dumbbell. The SPs represented by red and blue spheres correspond to first nearest neighbor migrations, the light green circles to rotations to a different member of the <110> family, and the pink circles rotations to <111> crowdion.

3.2 Screw Dislocation

Dislocations act as sinks for point defects [13], and thus it is generally expected that migration of point defects towards the dislocation core is more favorable, and energy barriers towards the dislocation have a smaller value. However, from Fig. 4 with the SP data obtained from SEAKMC, we find that the MEBs towards the dislocation core are not necessarily smaller than the values of other directions, and the migration energy variation exhibits a complex and non-linear dependence as a function of distance to the dislocation core. The change of the migration energy as a function of position for the different migration directions for a vacancy in a screw dislocation environment is presented in Fig. 4. In this figure, we are plotting the relative energy with respect to the bulk migration energy; we have done the same for all the figures in this section. The symmetry observed in Fig. 4 is related to the nature of the migration jumps. In the screw dislocation system, migration in the $[111]$ and $[\bar{1}\bar{1}\bar{1}]$ directions correspond to migration in the dislocation line direction. According to elasticity theory, the stress component in the dislocation line direction is zero, and thus we expect little change in the MEB in these directions as shown in Fig. 4. The migration to the $[1\bar{1}1]$ and $[1\bar{1}\bar{1}]$ nearest neighbors are mirrored by each other, as can be appreciated from Fig. 1, and hence their energy maps are mirrors of each other (the same applies for their negative

counterparts). The biggest change in the MEB value is in the $[11\bar{1}]$ and $[\bar{1}\bar{1}1]$ directions since they have the smallest components along the dislocation line direction. As expected the biggest difference in the saddle point energy is close to the dislocation core, and it decreases farther away from the core.

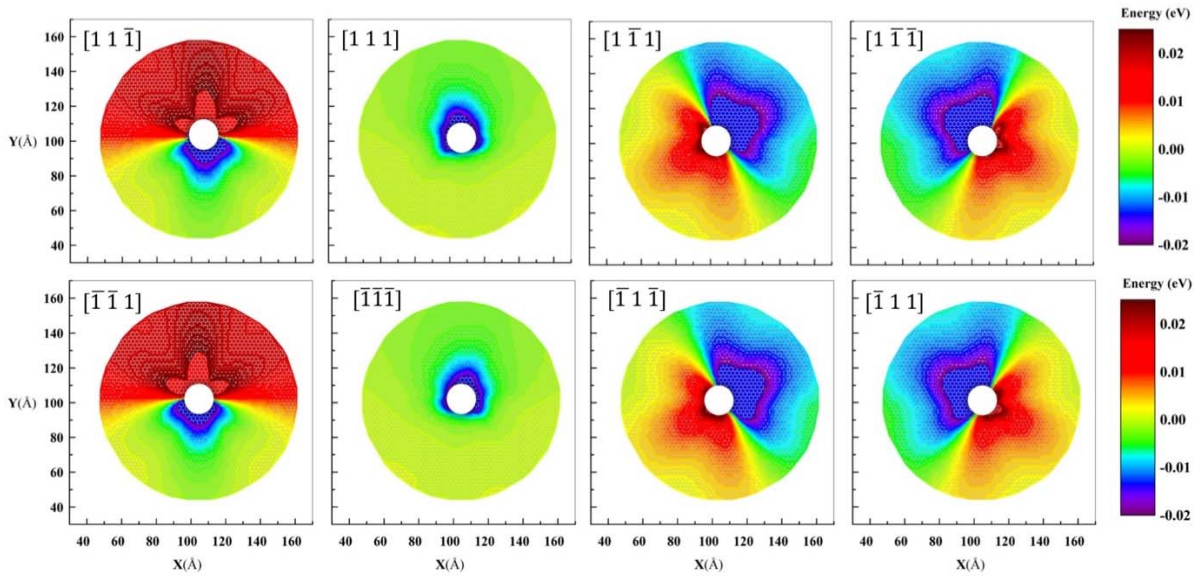

Figure 4: Migration energy maps of nearest neighbor migration for a vacancy in the presence of a screw dislocation.

The case of a $[\bar{1}01]$ dumbbell near a screw dislocation is shown in Fig. 5. In this case, the energy maps become more complicated because of the directional nature of the dumbbell. There are six different cases for the <110> dumbbell family and more details are given in the Supplementary Material section SM3. In this case, when a dumbbell migrates along the dislocation line, it interacts with not only the strain field in the migration direction, but also with other components of the strain field due to the directional nature of the defect. Just as in the vacancy case, the change in the migration energy is more pronounced close to the dislocation core. It is possible to observe that the difference in magnitude with respect to the bulk value is larger for the dumbbell case, since dumbbells introduces a larger distortion in the system than vacancies. Surprisingly, the energy maps for all directions look similar, there are in fact differences between the migration directions, but they do not display a particular behavior for each direction such as in the vacancy cases. The difference among different direction can be seen in the diffusion anisotropy figure (Fig. 11). The complexity to understand the change in MEB not only arises from the directional nature of the dumbbell, but also in that the migration mechanism involves both translation and rotation.

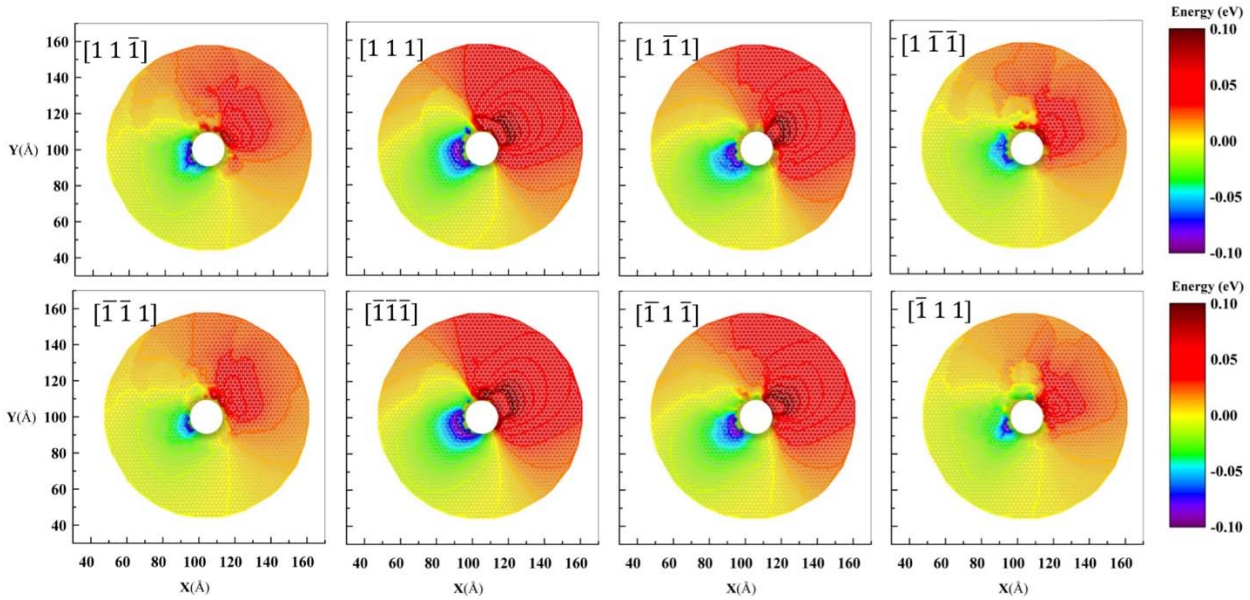

Figure 5: Migration energy barrier maps of different nearest neighbor migration directions for a $[\bar{1}01]$ dumbbell in the presence of a screw dislocation.

Fig. 6 shows the migration energy changes for all members of the <110> family migrating in the [111] direction. The symmetry relations observed in the figure are due to the direction of the dumbbells with respect to the dislocation core. This effect can be appreciated in the energy plots of the $[\bar{1}01]$ and $[0\bar{1}1]$ dumbbells, which are mirrors of each other; a similar relationship is found between the [101] and [011] dumbbells. The directions containing a negative index have no components in the dislocation line direction, while the directions with all positive indices have components in the dislocation line direction. This results in the directions with all positive indices having a smaller change in the migration energy compared to the directions with a negative index, since the stress component along the dislocation line is negligible, which results in essentially no interaction with the dumbbell in this particular direction.

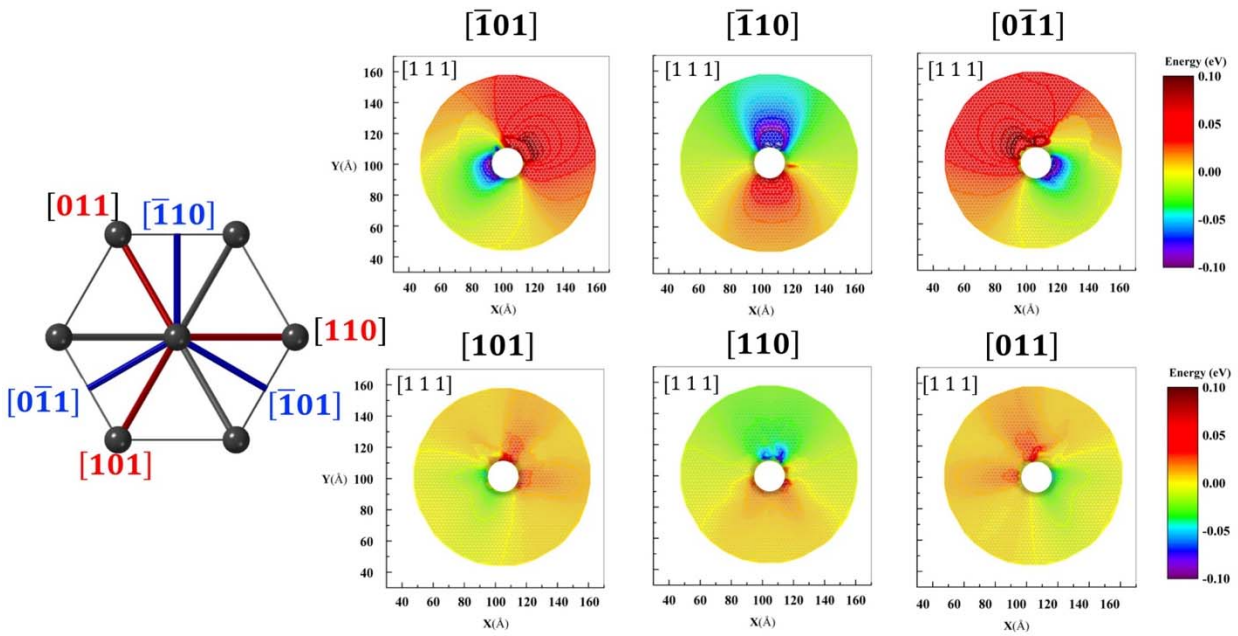

Figure 6: Migration energy barrier maps for different members of the <110> dumbbell family in the [111] migration direction.

As it was mentioned in section 4.1 we also found saddle points that correspond to rotation from one <110> type dumbbell to a different member of the <110> family. In figure 7 we show the change of the energy barrier for a rotation of [101] dumbbell as a function of position to a screw dislocation. The plots show that there is a significant dependence of rotation energies with respect of position. There are regions where the rotation energies are reduced compared with the bulk case, resulting in faster rotations near dislocation core, such as the bulk and green regions in the bottom two figures of Fig. 7. In comparison, certain regions lead to slower rotation, e.g. the red regions in bottom two figures of Fig. 7, also indicating that rotations to particular dumbbell configuration occur more often than other directions. Compared with the results of first near neighbor jump, the presence of dislocations not only influence the rate of jumping but also the rate of dumbbell rotations, resulting in complex defect dynamics that are challenging for conventional techniques and methods.

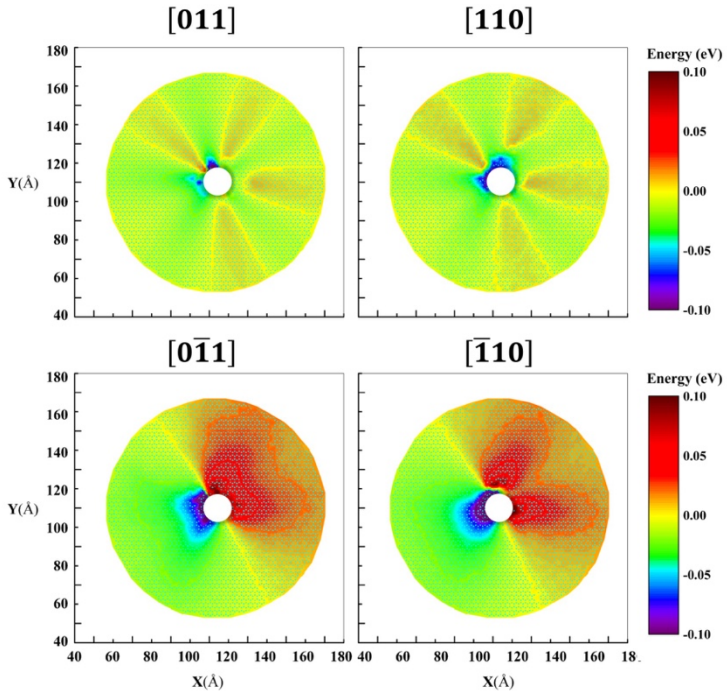

Figure 7: Migration energy barrier for a [101] dumbbell rotation to different members of the <110> family near a screw dislocation.

3.3 Edge Dislocation

Fig. 8 shows the relative migration energies as a function of position for the different migration directions of a vacancy in an edge dislocation environment. Because of the slip system of an edge dislocation, there are no longer migration jumps in the dislocation line directions. In comparison, the migration jumps in the [111] and $[\bar{1}\bar{1}\bar{1}]$ directions correspond to migration along the glide direction. In these directions, the effects of the compressive and tensile stress field in the different regions of the edge dislocation are more evident compared with changes in migration energy among all migration directions ($[\bar{1}1\bar{1}], [\bar{1}11], [1\bar{1}1], [1\bar{1}\bar{1}], [11\bar{1}]$ and $[\bar{1}\bar{1}1]$). The symmetry relations are similar to those of the screw-vacancy case; the mirror relationship between $[1\bar{1}1]$ and $[1\bar{1}\bar{1}]$ still holds and their energy maps are again mirrors of each other.

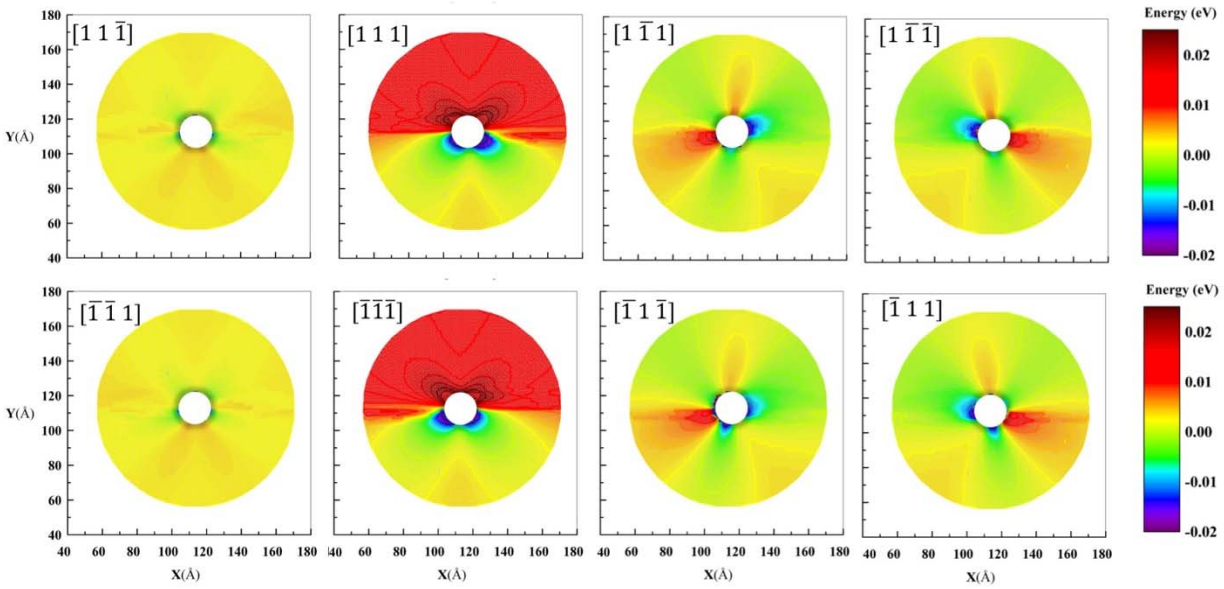

Figure 8: Migration energy barrier maps of different nearest neighbor migration directions for a vacancy in the presence of an edge dislocation.

Fig. 9 shows the migration energies of an $[\bar{1}01]$ dumbbell near an edge dislocation. Just as with the screw case, the SP energy maps strongly depend on the configuration of the dumbbell. The mirror symmetry relationship observed in the vacancy case for the $[1\bar{1}1]$ and $[1\bar{1}\bar{1}]$ directions are broken by the directional nature of the dumbbell (except for the $[\bar{1}10]$ and $[110]$ dumbbell configurations where mirror symmetry still exists, see Supplementary Material section SM4). It can be observed that for both screw and edge dislocations, the change in migration energy for dumbbells is greater than for vacancies due to their larger distortion in the lattice. For the vacancy case, we have attempted to relate the migration energies to the strain/stress field by fitting the SP energies to analytical expressions, but none of them yield reasonable agreement with the SP data. The trends displayed in the energy maps between the screw and edge dislocations are significantly different, partially due to the strain fields generated by each type of dislocation.

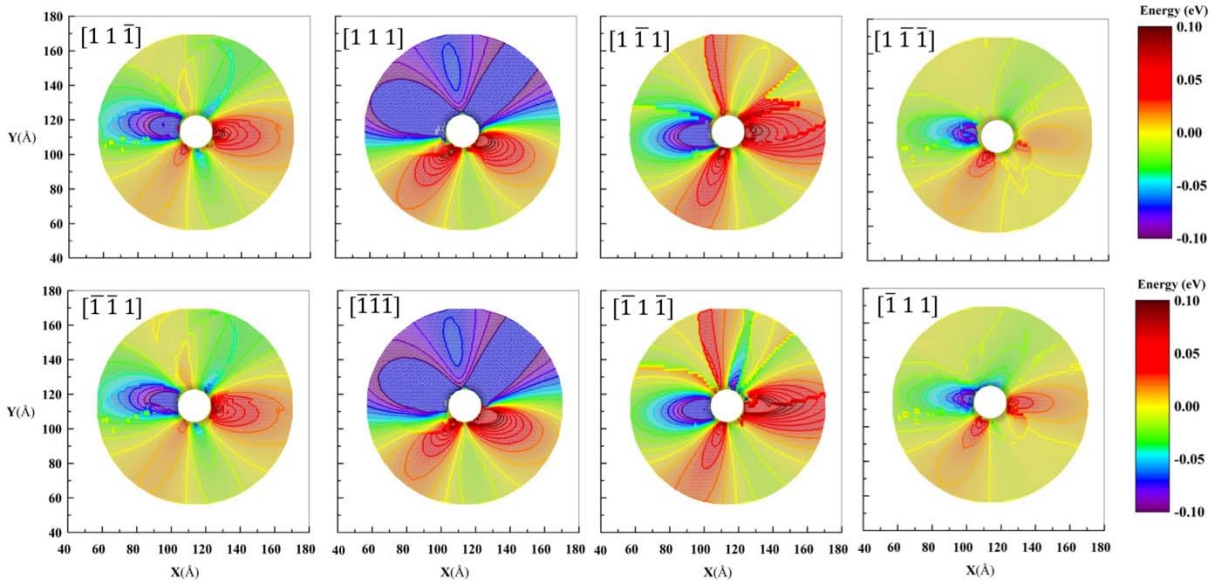

Figure 9: Migration energy barrier maps of different nearest neighbor migration directions for a $[\bar{1}01]$ dumbbell in the presence of an edge dislocation.

In figure 10 we show the change of the energy barrier for a rotation of [101] dumbbell as a function of position near an edge dislocation. Similar to the screw dislocation case, these plots show rotations energies have a strong dependence on the position of the defect. Particularly, in the bottom two figures we can observe rotations get slower as we approach the dislocation core from the upper half but become faster if we approach the dislocation from the lower half of the system. Compared with the two upper figures (in Fig. 10), we can see that rotations of [011] and [110] dumbbell occur more often in the areas that correspond to slower rotations for $[0\bar{1}1]$ and $[\bar{1}10]$.

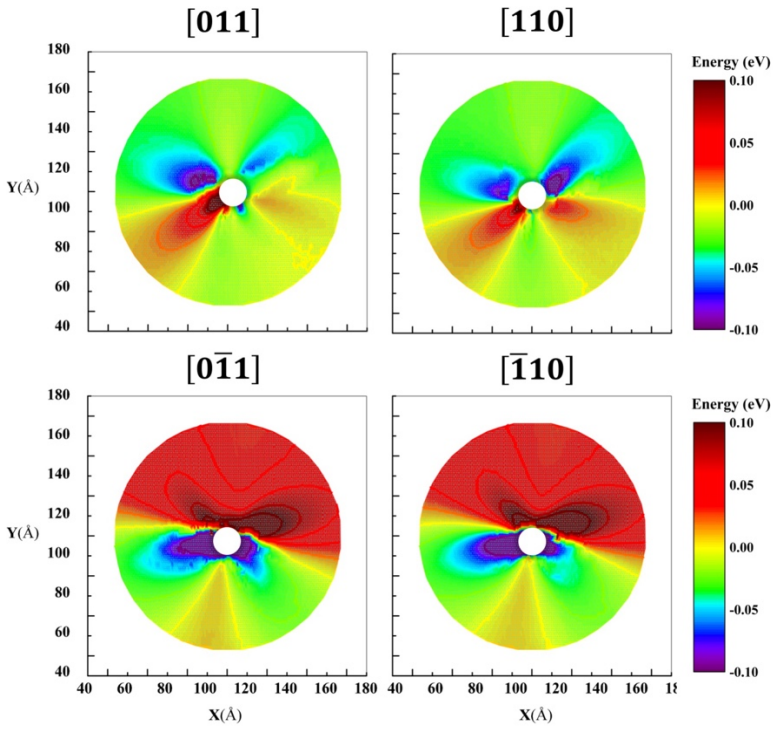

Figure 10: Migration energy barrier for a [101] dumbbell rotation to different members of the <110> family near an edge dislocation.

3.4 Diffusion Anisotropy

In the bulk, point defect migration exhibits a random walk motion; the presence of the dislocation changes the SP configurations and energies, resulting in a certain migration direction having a higher probability than the other directions. This leads to anisotropic diffusion. To analyze the diffusion anisotropy, we have taken the difference between the smallest and largest SP energy values as a function of position with respect of the dislocation core for both screw and edge dislocations as shown in Fig. 11. In general, dumbbell defects have a higher anisotropy of diffusion due to the directional nature of the defect and the larger strain it introduces. The anisotropy of diffusion leads to more complex diffusion paths. Particularly, the strong diffusion anisotropy of dumbbells near both edge and screw dislocations indicates they will likely have preferred migration paths.

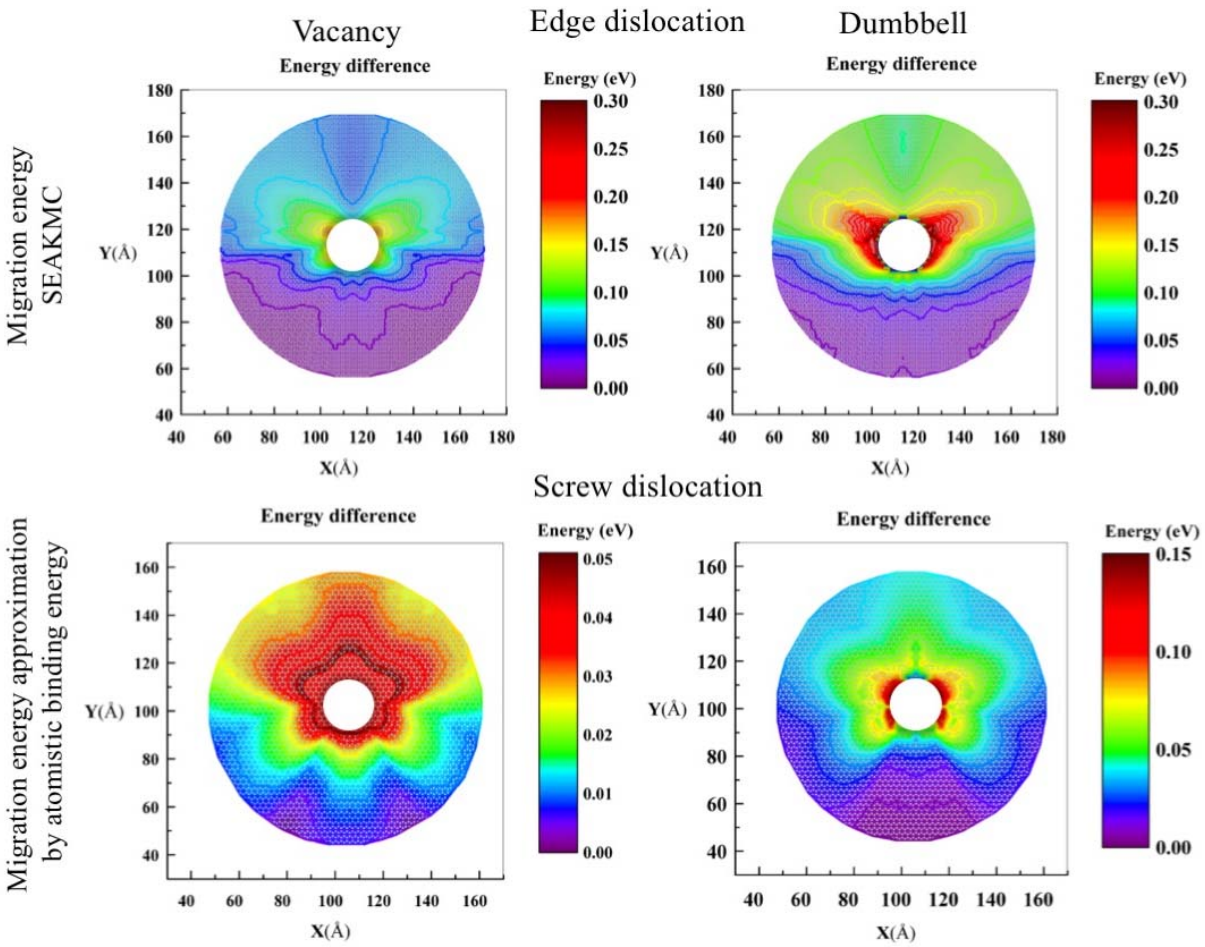

Figure 11: Anisotropy of diffusion for vacancies and dumbbells for an edge and screw dislocation.

From the SP searches we can also obtain the direction of the SP with the lowest energy barrier at each position and construct the "most probable migration maps". This type of plots permits visualization of what would be the most probable migration of a point defect as a function of position with respect to the dislocation core. These directions will be more often followed at low temperatures, where the effect of the difference between energy barriers is more prominent. As the temperature rises, the migration of point defects approaches random walk diffusion. The most probable migration maps for a vacancy and a dumbbell in a screw dislocation environment are given in Fig. 12, in which the vacancy case is in good agreement with the results of Sivak *et al.* [29,30] where the strain field is small. In contrast, our dumbbell results are dramatically different from Sivak *et al.* [29,30]. Fig 12b is the most probable migration map for the $[\bar{1}10]$ dumbbell. It should be noted that there is a different map for each different member of the <110> dumbbell family. Since the migration mechanism involves translation and rotation at every jump the most probable path, the overall most probable path is determined by the most probable maps for all

dumbbell configurations. The anisotropy of diffusion of a point defect at the saddle point can influence the sink strength of dislocations [51-53]. Recently, Carpentier et. al [54] and Vattré et al. [55] estimated the DPDI using the elastic dipole tensors [56,57] at the saddle point configurations instead of calculating the dipole tensor at the local minimum configurations. Carpentier et al. concluded that the diffusion anisotropy is not captured by dipole tensor calculated at the local minimum configurations, and complex defect trajectories can only be obtained through the saddle point configuration. The saddle point anisotropy increases the sink strength and bias and leads to a biased sink behavior for a cavity.

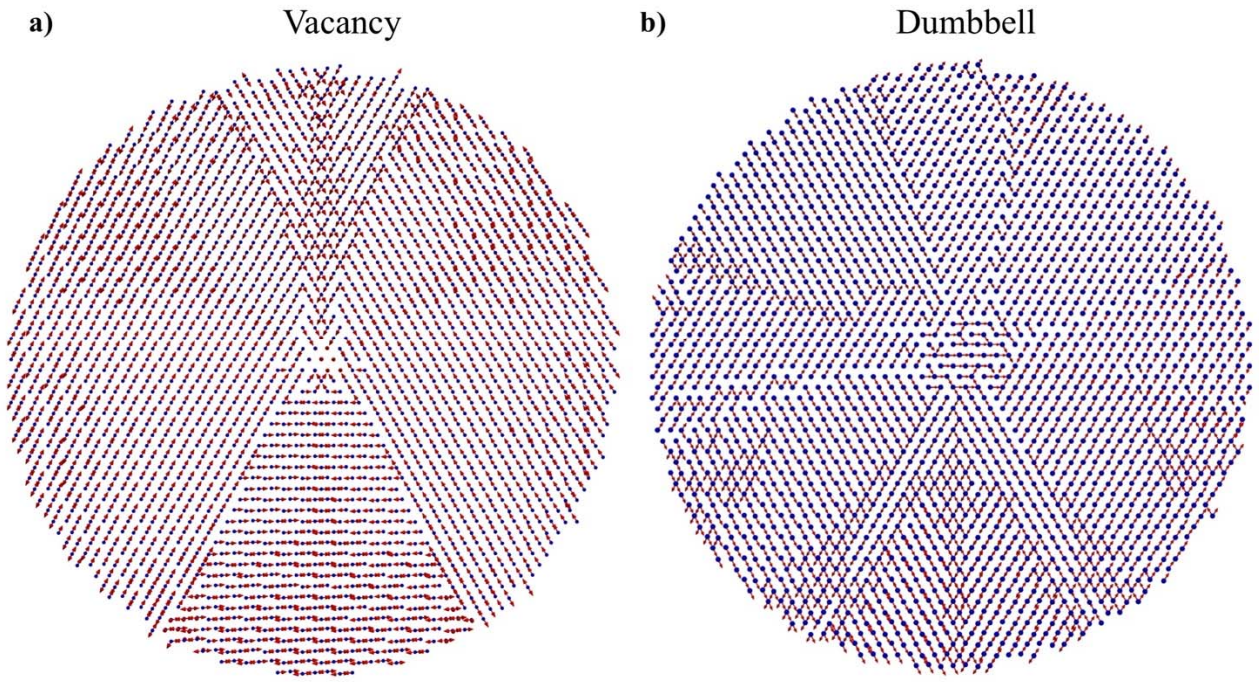

Figure 12: (a) Most probable migration map for a vacancy (b) most probable migration map for a $[\bar{1}10]$ dumbbell, in a screw dislocation environment.

3.5 KMC Simulations of Defect Trajectories

The data obtained in this study can be used as an input for kinetic Monte Carlo (KMC) simulations, allowing realistic migration paths. For each position of interest, we performed 10,000 KMC simulations. We found that the diffusion of a defect near dislocations is highly anisotropic and strongly correlated, greatly deviating from a simple symmetric random walk. This correlated behavior is shown in Fig. 13, where we have plotted several migration trajectories of dumbbell defects for both screw and edge dislocations and compared with random walk trajectories. the Using KMC we have identified the regions in which each type of defect is more efficiently absorbed by the dislocation core. We have

obtained the time required by each defect to be absorbed by the dislocation and divided it by the time required to reach the dislocation core by a simple symmetric random walk. This ratio denotes the deviations of the migration behavior from a random walk diffusion by the presence of the dislocation. We show the absorption time for a vacancy and dumbbell to reach the dislocation core of a screw dislocation with the obtained barriers and with a random walk respectively in Fig 13e and Fig.13f. Blue zones denote regions where vacancies are absorbed more efficiently, and red zones regions where dumbbells are more efficiently absorbed. Interestingly, we find that the region where a vacancy is absorbed more efficiently coincides with the compressive field of the dislocations, and dumbbells must migrate to a tensile zone to be able to find a path to reach the dislocation core, as can be seen from the trajectories. This behavior will be more accentuated at low temperature and become less prominent as temperature increases (e.g. room temperature), for this reason we performed the simulations at T=100K and enhance the preference between barriers. As it has been shown, the accurate migration energy data used in the KMC simulations has a deep impact on the defect trajectory, thus allowing a realistic estimation of important parameters such as of the lifetime of point defects (how long it takes to be absorbed by the dislocation), sink strength and dislocation bias. The diffusion mechanism of dumbbells is rather complex, involving translation, rotations and the effect of different dumbbell configuration. The individual migration energy maps change drastically for different directions and do not show a direct relationship with the strain field of dislocations. However, the overall effects from all these mechanisms and all dumbbell configurations produce diffusion trajectories that are related to the strain fields of dislocations. For instance, the 3-fold symmetry is recovered for the screw dislocation and the effects of the compressive/tensile regions are appreciated in the edge case (Fig. 13). These observations may provide basis to allow the development of simple models to describe the dynamics of point defects near dislocations in materials.

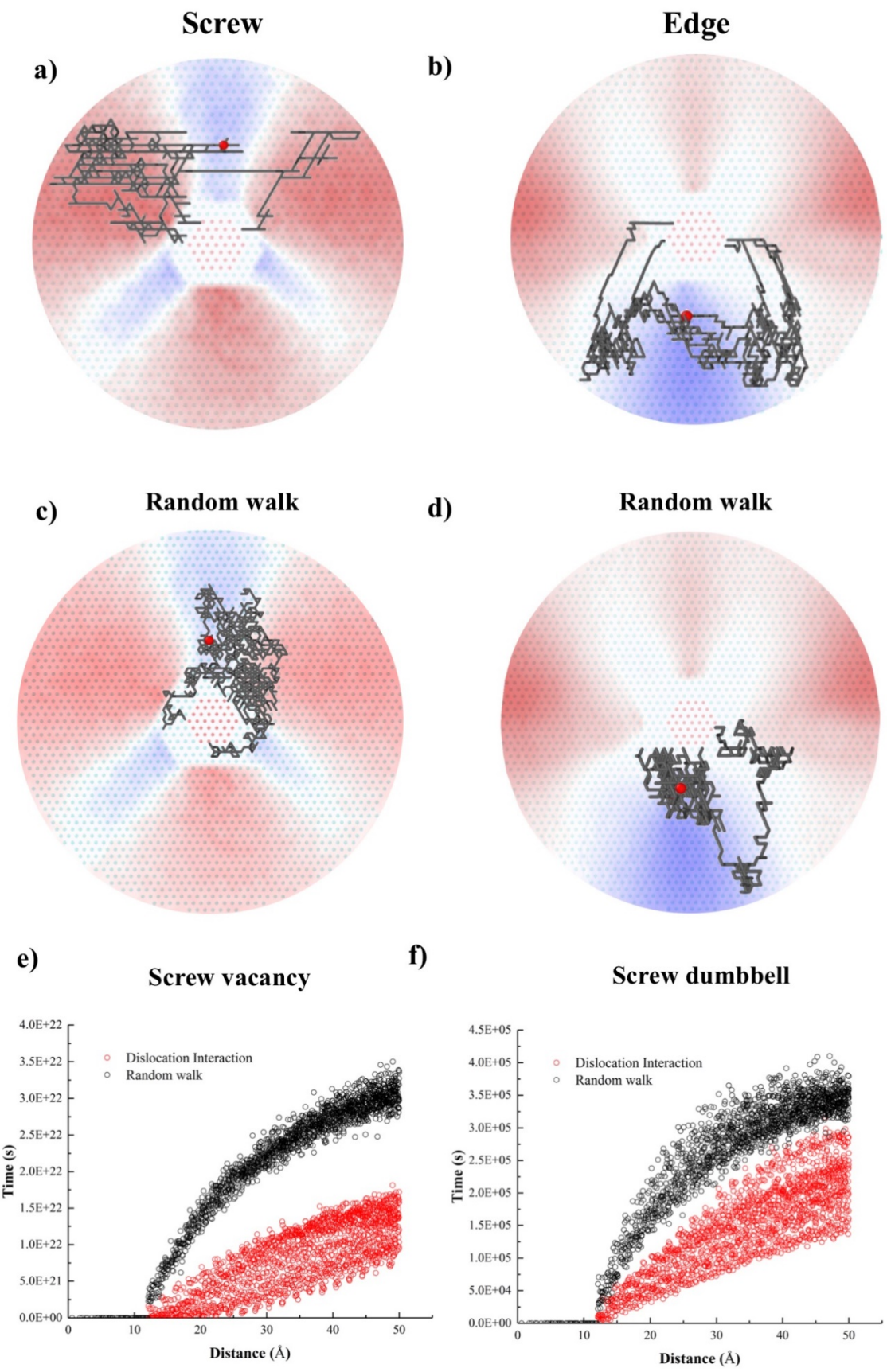
Screw
Edge
a)
b)
c)
Random walk
d)
Random walk
e)
Screw vacancy
f)
Screw dumbbell
Dislocation Interaction
Random walk
Time (s)
Distance (Å)
4.0E+22
3.5E+22
3.0E+22
2.5E+22
2.0E+22
1.5E+22
1.0E+22
5.0E+21
0.0E+00
4.5E+05
4.0E+05
3.5E+05
3.0E+05
2.5E+05
2.0E+05
1.5E+05
1.0E+05
5.0E+04
0.0E+00
0
10
20
30
40
50

Figure 13: Dumbbell migration path around a (a) screw (b) edge dislocation, (c) random walk of a dumbbell in a screw dislocation, (d) random walk of a dumbbell in an edge dislocation. The large red sphere represents the dumbbell starting position. The dislocation core is represented by the red colored atoms. (e) Time of absorption for a vacancy near a screw dislocation, and for random walk diffusion (f) time of absorption for a dumbbell near a screw dislocation and for random walk diffusion.

4. Conclusions

In this work, we have presented the actual MEBs and SP configurations for a vacancy and a dumbbell as a function of position in the presence of a (screw/edge) dislocation. The SEAKMC approach captures the complexity of the migration mechanisms of point defects, and the effect of different local atomic environments introduced by dislocations, as we have shown in the first nearest neighbor migration and rotations energy barrier plots. Based on the migration energy maps, we find that the atomistic processes of the dislocation-point defect interaction (for both vacancy and interstitial) are highly anisotropic and correlated. The anisotropy of diffusion is appreciated with the "most probable migration" maps and by defect trajectories. For instance, a dumbbell around an edge or screw dislocation must escape the compressive region of the dislocations to be absorbed. This study provides critical information on how to capture the real dynamics of point defects near complex defects (e.g. dislocations, dislocation loops, grain boundaries) and the results in this study can be used as an input for coarser scale models, such as mean field rate theory. This study also provides the basis for investigations of material properties that depend on the interaction between dislocations and point defects, such as void swelling and creep, that are of interest for various practical applications.

Acknowledgements

The authors would like to thank Dr. Roger Stoller for his useful comments and suggestions on the manuscript. The research is sponsored by the U.S. Department of Energy Nuclear Energy University Program (project number 14-6346) under contract number DE-NE0008271. This research used resources of the National Energy Research Scientific Computing Center, a DOE Office of Science User Facility supported by the Office of Science of the U.S. Department of Energy under Contract No. DE-AC02-05CH11231 and the Newton High Performance Computing program at the University of Tennessee.

References

[1] C. Azevedo, A review on neutron-irradiation-induced hardening of metallic components, *Engineering Failure Analysis*, 18, 1921 (2011).

[2] A. Brailsford and R. Bullough, The theory of sink strengths, *Phil. Trans. of the R. Soc. of London A*, 302, 87 (1981).

[3] D. Braski, H. Schroeder, and H. Ullmaier, The effect of tensile stress on the growth of helium bubbles in an austenitic stainless steel, *J. Nucl. Mater.*, 83, 265 (1979).

[4] G. Greenwood, A. Foreman, and D. Rimmer, The role of vacancies and dislocations in the nucleation and growth of gas bubbles in irradiated fissile material, *J. Nucl. Mater.*, 1, 305 (1959).

[5] D. R. Trinkle and C. Woodward, The chemistry of deformation: How solutes soften pure metals, *Science*, 310, 1665 (2005).

[6] H. Ullmaier, The influence of helium on the bulk properties of fusion reactor structural materials, *Nucl. Fusion*, 24, 1039 (1984).

[7] D. Hull and D. J. Bacon, *Introduction to dislocations* (Butterworth-Heinemann, 2001).

[8] W. Wolfer and M. Baskes, Interstitial solute trapping by edge dislocations, *Acta Metall.*, 33, 2005 (1985).

[9] D. Hull and D. J. Bacon, *Introduction to dislocations* (Pergamon Press Oxford, 1984), Vol. 257.

[10] J. G. Harper, L. A. Shepard, and J. E. Dorn, Creep of aluminum under extremely small stresses, *Acta Metall.*, 6, 509 (1958).

[11] A. H. Cottrell and B. Bilby, Dislocation theory of yielding and strain ageing of iron, *Proc. of the Phys. Soc.. Sect. A*, 62, 49 (1949).

[12] S. Hu and L. Chen, Solute segregation and coherent nucleation and growth near a dislocation—a phase-field model integrating defect and phase microstructures, *Acta Mater.*, 49, 463 (2001).

[13] G. S. Was, *Fundamentals of radiation materials science: metals and alloys* (Springer, 2016).

[14] D. R. Olander, Fundamental aspects of nuclear reactor fuel elements, US Energy Research and Development Administration Report TID-26711-P1 (1976).

[15] C. Cawthorne and E. Fulton, Voids in irradiated stainless steel, *Nature*, 216, 575 (1967).

[16] P. Okamoto and L. Rehn, Radiation-induced segregation in binary and ternary alloys, *J. Nucl. Mater.*, 83, 2 (1979).

[17] H. Wiedersich, P. Okamoto, and N. Q. Lam, A theory of radiation-induced segregation in concentrated alloys, *J. Nucl. Mater.*, 83, 98 (1979).

[18] W. Wolfer, Correlation of radiation creep theory with experimental evidence, *J. Nucl. Mater.*, 90, 175 (1980).

[19] L. Mansur, Theory and experimental background on dimensional changes in irradiated alloys, *J. Nucl. Mater.*, 216, 97 (1994).

[20] B. Singh, A. Foreman, and H. Trinkaus, Radiation hardening revisited: role of intracascade clustering, *J. Nucl. Mater.*, 249, 103 (1997).

[21] H. Trinkaus, B. Singh, and A. Foreman, Segregation of cascade induced interstitial loops at dislocations: possible effect on initiation of plastic deformation, *J. Nucl. Mater.*, 251, 172 (1997).

[22] K. K. Adepalli, J. Yang, J. Maier, H. L. Tuller, and B. Yildiz, Tunable Oxygen Diffusion and Electronic Conduction in SrTiO3 by Dislocation-Induced Space Charge Fields, *Adv. Funct. Mater.*, 27, (2017).

[23] E. Navickas *et al.*, Dislocations Accelerate Oxygen Ion Diffusion in La0. 8Sr0. 2MnO3 Epitaxial Thin Films, *ACS nano*, 11, 11475 (2017).

[24] M. Nastar and F. Soisson, *Comprehensive Nuclear Materials* (Elsevier, New York, 2012) Cahp. 1.18, pp. 471-496.

[25] B. Bilby, On the interactions of dislocations and solute atoms, *Proc. of the Phys. Soc. A*, 63, 191 (1950).

[26] A. Cottrell, Report of a Conference on Strength of Solids, *Phys. Soc., London*, 30, (1948).

[27] E. Hayward, C. Deo, B. P. Uberuaga, and C. N. Tomé, The interaction of a screw dislocation with point defects in bcc iron, *Philos. Mag.*, 92, 2759 (2012).

[28] V. Shastry and T. D. De La Rubia, Interaction between point defects and edge dislocation in BCC iron, *Trans. Am. Soc. of Mech. Eng. J. of Eng. Mater. and Tech.*, 121, 126 (1999).

[29] A. Sivak, V. Chernov, N. Dubasova, and V. Romanov, Anisotropy migration of self-point defects in dislocation stress fields in BCC Fe and FCC Cu, *J. Nucl. Mater.*, 367, 316 (2007).

[30] A. Sivak, V. Romanov, and V. Chernov, Diffusion of self-point defects in body-centered cubic iron crystal containing dislocations, *Crystallography reports*, 55, 97 (2010).

[31] G. Henkelman, G. Jóhannesson, and H. Jónsson, in *Theoretical Methods in Condensed Phase Chemistry* (Springer, 2002), pp. 269.

[32] G. Henkelman and H. Jónsson, Improved tangent estimate in the nudged elastic band method for finding minimum energy paths and saddle points, *The J. of Chem. Phys.*, 113, 9978 (2000).

[33] G. Henkelman, B. P. Uberuaga, and H. Jónsson, A climbing image nudged elastic band method for finding saddle points and minimum energy paths, *The J. of Chem. Phys.*, 113, 9978 (2000).

[34] G. Henkelman and H. Jónsson, A dimer method for finding saddle points on high dimensional potential surfaces using only first derivatives, *The J. of Chem. Phys.*, 111, 7010 (1999).

[35] H. Xu, R. E. Stoller, L. K. Béland, and Y. N. Osetsky, Self-evolving atomistic kinetic monte carlo simulations of defects in materials, *Comput. Mater. Sci.*, 100, 135 (2015).

[36] N. Castin and L. Malerba, Calculation of proper energy barriers for atomistic kinetic Monte Carlo simulations on rigid lattice with chemical and strain field long-range effects using artificial neural networks, *The J. of Chem. Phys.*, 132, 074507 (2010).

[37] F. Djurabekova, R. Domingos, G. Cerchiara, N. Castin, E. Vincent, and L. Malerba, Artificial intelligence applied to atomistic kinetic Monte Carlo simulations in Fe–Cu alloys, *Nucl. Instrum. and Methods in Phys. Res. Sect. B*, 255, 8 (2007).

[38] F. Soisson, C. Becquart, N. Castin, C. Domain, L. Malerba, and E. Vincent, Atomistic Kinetic Monte Carlo studies of microchemical evolutions driven by diffusion processes under irradiation, *J. Nucl. Mater.*, 406, 55 (2010).

[39] R. Domingos, G. Cerchiara, F. Djurabekova, and L. Malerba, Artificial intelligence applied to simulation of radiation damage in ferritic alloys, *Applied Artificial Intelligence, Genova, Italy*, 29 (2006).

[40] L. K. Béland, Y. N. Osetsky, R. E. Stoller, and H. Xu, Kinetic activation–relaxation technique and self-evolving atomistic kinetic Monte Carlo: Comparison of on-the-fly kinetic Monte Carlo algorithms, *Comput. Mater. Sci.*, 100, 124 (2015).

[41] H. Xu, Y. N. Osetsky, and R. E. Stoller, Simulating complex atomistic processes: On-the-fly kinetic Monte Carlo scheme with selective active volumes, *Phys. Rev. B*, 84, 132103 (2011).

[42] H. Xu, Y. N. Osetsky, and R. E. Stoller, Self-evolving atomistic kinetic Monte Carlo: fundamentals and applications, *J. Phys.: Condens. Matter*, 24, 375402 (2012).

[43] H. Xu, R. E. Stoller, Y. N. Osetsky, and D. Terentyev, Solving the Puzzle of⟨ 100⟩ Interstitial Loop Formation in bcc Iron, *Phys. Rev. Lett.*, 110, 265503 (2013).

[44] J. Weertman and J. R. Weertman, Elementary dislocation theory, (New York, Oxford University Press, 1966).

[45] G. Ackland, M. Mendelev, D. Srolovitz, S. Han, and A. Barashev, Development of an interatomic potential for phosphorus impurities in α-iron, *J. Phys.: Condens. Matter*, 16, S2629 (2004).

[46] S. Chiesa, M. Gilbert, S. Dudarev, P. Derlet, and H. Van Swygenhoven, The non-degenerate core structure of a ½⟨ 111⟩ screw dislocation in bcc transition metals modelled using Finnis–Sinclair potentials: The necessary and sufficient conditions, *Phil. Mag.*, 89, 3235 (2009).

[47] Y. N. Osetsky and D. J. Bacon, An atomic-level model for studying the dynamics of edge dislocations in metals, *Modelling and Simulation in Mater. Sci. and Eng.*, 11, 427 (2003).

[48] A. Heyden, A. T. Bell, and F. J. Keil, Efficient methods for finding transition states in chemical reactions: Comparison of improved dimer method and partitioned rational function optimization method, *The J. of Chem. Phys.,* 123, 224101 (2005).

[49] J. Kästner and P. Sherwood, Superlinearly converging dimer method for transition state search, *The J. of Chem. Phys.*, 128, 014106 (2008).

[50] R. Malek and N. Mousseau, Dynamics of Lennard-Jones clusters: A characterization of the activation-relaxation technique, *Phys. Rev. E*, 62, 7723 (2000).

[51] I.W. Chen, Anisotropic diffusion of point defects to edge dislocations, *J. Nucl. Mater.*, 125, 52 (1984).

[52] P. Dederichs and K. Schroeder, Anisotropic diffusion in stress fields, *Phys. Rev. B*, 17, 2524 (1978).

[53] C. Tomé, H. Cecatto, and E. Savino, Point-defect diffusion in a strained crystal, *Phys. Rev. B*, 25, 7428 (1982).

[54] D. Carpentier, T. Jourdan, Y. Le Bouar, and M.C. Marinica, Effect of saddle point anisotropy of point defects on their absorption by dislocations and cavities, *Acta Mater.*, 136, 323 (2017).

[55] A. Vattré, T. Jourdan, H. Ding, M.C. Marinica, and M. Demkowicz, Non-random walk diffusion enhances the sink strength of semicoherent interfaces, *Nature communications*, 7, 10424 (2016).

[56] E. Clouet, C. Varvenne, and T. Jourdan, Computational Materials Science 147, 49 (2018).

[57] C. Varvenne and E. Clouet, Elastic dipoles of point defects from atomistic simulations, *Phys. Rev. B*, 96, 224103 (2017).